

Experimental study on a broadband omnidirectional electromagnetic absorber

This article has been downloaded from IOPscience. Please scroll down to see the full text article.

2011 J. Opt. 13 085103

(<http://iopscience.iop.org/2040-8986/13/8/085103>)

View [the table of contents for this issue](#), or go to the [journal homepage](#) for more

Download details:

IP Address: 202.204.81.80

The article was downloaded on 15/07/2011 at 16:00

Please note that [terms and conditions apply](#).

Experimental study on a broadband omnidirectional electromagnetic absorber

Jiao Zhou, Xiaobing Cai¹, Zheng Chang and Gengkai Hu¹

School of Aerospace Engineering, Beijing Institute of Technology, Beijing 100081, People's Republic of China

E-mail: caixiaobing@bit.edu.cn and hugeng@bit.edu.cn

Received 10 March 2011, accepted for publication 23 June 2011

Published 14 July 2011

Online at stacks.iop.org/JOpt/13/085103

Abstract

A broadband omnidirectional electromagnetic absorber is constructed with traditional materials including silicon powder, polyethylene and a mixture of water and ethanol. Variation of the dielectric constant in the radial direction of the device is realized by gradually changing the fraction of silicon powder and polyethylene, and the absorbing core is made by mixing water and ethanol. By placing the device into a parallel metallic board and under electromagnetic illumination, we demonstrate that the trajectories of the incident waves fall into the core at both 9.0 and 10.0 GHz, as predicted by numerical simulation. Since the device is constructed without a resonant element, it can be expected to have a broadband nature.

Keywords: black hole, omnidirectional electromagnetic absorber, metamaterial, transformation optics

(Some figures in this article are in colour only in the electronic version)

1. Introduction

The transformation method provides an unprecedented way to control wave propagation with a spatial distribution of materials [1–9], especially with the development of electromagnetic metamaterials [10–17]. An interesting example is the omnidirectional electromagnetic absorber, initially proposed by Narimanov and Kildishev [18]. By spatially varying the dielectric constant, a beam of electromagnetic waves can be guided to fall into a region where the energy can be harvested or absorbed. An experimental demonstration was conducted recently by Cheng *et al* with a non-resonant shell and a resonant absorbing core based on a printed circuit technique [19]. The transformation version of this omnidirectional electromagnetic absorber was recently examined by Lu *et al* [20]. Although the idea proposed by Narimanov and Kildishev [18] can be applied to a broadband frequency range, using the resonant core may limit the frequency band for this device. In this paper, we will show that by careful design an omnidirectional electromagnetic absorber can be constructed with traditional materials such as silicon powder, polymeric material and a mixture of water and ethanol. This

paper will be arranged as follows: after a recall of the theory of an omnidirectional electromagnetic absorber, the material design of the device is explained in section 2, the detailed experimental implementation of the proposed model will be given in section 3. A comparison with the numerical simulation will also be provided, followed by some conclusions.

2. Design of an omnidirectional electromagnetic absorber

Narimanov and Kildishev [18] proposed an optical omnidirectional absorber with a shell controlling the ray trajectory and a core absorbing the wave energy; the permittivity of the device fits the following expression [18]:

$$\varepsilon(r) = \begin{cases} \varepsilon_0 \varepsilon_c, & r < R_c \\ \varepsilon_0 \left(\frac{R}{r}\right)^n, & R_c < r < R, \\ \varepsilon_0, & r > R, \end{cases} \quad (1)$$

where R is the outer radius of the device, R_c is the radius of the absorbing core, ε_0 is the dielectric constant of free space and ε_c is the relative complex permittivity of the core. Depending

¹ Authors to whom any correspondence should be addressed.

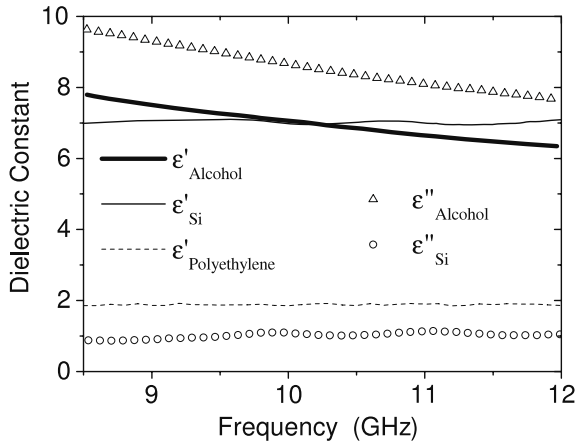


Figure 1. The measured permittivity of the alcohol with water and ethanol at a volume ratio of 100:240 (bold line and triangles) and the silicon powder (thin line and circles).

on n , an incident wave can be attracted into or pushed away from the core. A beam will be attracted into the core of the device if $n \geq 2$, a larger value of n implies that the system is more attractive and a beam will fall more rapidly into the core, while $n = 2$ denotes the critical condition in which the beam can be captured. In our experimental setup, $n = 2$ is chosen throughout the work. The outer radius of the device R can be chosen arbitrarily; however, from equation (1), a large R will lead to a high permittivity for the device, which will pose difficulties for subsequent material realization. So in the following experiment we choose $R = 120$ mm. After setting up the structural parameters of the shell, we then need to define a damping core to absorb the fallen beam; the impedance of the shell and core boundary must be matched to avoid reflection. If the real part of the dielectric constant of the core is denoted by $\text{Re}(\epsilon_c)$, according to equation (1) the impedance-matched condition at the shell–core boundary defines the radius of the core as

$$R_c = R \sqrt{\frac{1}{\text{Re}(\epsilon_c)}}. \quad (2)$$

The dielectric constant of the core should also have a large imaginary value in order to absorb the beam, thus a high damping material is necessary. Inspired by a microwave oven that generates heats by interaction between microwaves and water, one is readily aware that water is an ideal medium for absorbing electromagnetic energy. To further maintain the impedance-matched condition at the core–shell interface, ethanol is selected as an additive to water in order to tune the permittivity of the mixture. After many tests, a mixture of water and ethanol at a ratio 100:240 is chosen, and its effective permittivity is measured with a vector network analyzer at 14 °C; the results are illustrated by the bold line and triangles in figure 1. It is seen that the alcohol has a large damping factor, as shown by the imaginary part of the dielectric constant illustrated by the triangles. At the frequency range of interest, say 9–12 GHz, the permittivity of the mixture can be approximated as a constant, i.e. $\epsilon_c = 7 + 8.5i$.

Once the core material is fixed, we have to construct the shell with an effective permittivity satisfying equation (1). The

basic idea is to use a bilayered medium; for a long wavelength approximation the electric response of a bilayered medium can be well characterized by an equivalent medium with the effective permittivity

$$\epsilon_{\text{eff}} = (\epsilon_a h_a + \epsilon_b h_b) / h, \quad (3)$$

where ϵ_a , ϵ_b and h_a , h_b are, respectively, the permittivity and thickness of layer one and layer two, and $h = h_a + h_b$ denotes the total thickness. By changing the thickness ratio of the two layers along the radial direction, the effective permittivity of the bilayered medium can be tailored to satisfy equation (1).

According to equation (3), the adjustable range of the effective dielectric constant of the bilayered medium is between ϵ_a and ϵ_b . Since the core material is already fixed with a real part of the dielectric constant $\text{Re}(\epsilon_c) = 7$, we need to find a material which also possesses a matched dielectric constant to reduce the reflection at the interface of the core and shell. Silicon powder is an eligible candidate with a real dielectric constant $\epsilon_3 = 7.0$ for a normal depositing state. The thin line and circles in figure 1 show the measured dielectric constant of the silicon powder. It is found that the dielectric constant of the silicon powder is almost constant, $\epsilon_3 = 7.0 + 1.0i$, over a large measured frequency range. For the bilayered medium which makes up the shell of the device, we choose one layer as silicon powder and the other layer as polyethylene with a dielectric constant of $\epsilon_2 = 1.85$ and low loss. To tailor the effective dielectric constant ϵ_{eff} to follow equation (1), we will vary the thickness of the polyethylene plate $h_2(r)$ as a function of the radius of the device. $h_2(r)$ fits the following equation:

$$\epsilon_{\text{eff}}(r)h_0 = \epsilon_3 h_3(r) + \epsilon_2 h_2(r) = (R/r)^2 h_0, \quad (4)$$

where ϵ_3 , ϵ_2 and $h_3(r) = h_0 - h_2(r)$, $h_2(r)$ are, respectively, the permittivity and radius dependent thickness of the silicon powder and polyethylene. Equation (4) yields the radius dependent thickness of the polyethylene plate

$$h_2(r) = \frac{(\epsilon_3 r^2 - R^2)h_0}{(\epsilon_3 - \epsilon_2)r^2}. \quad (5)$$

Since $h_2(r)$ cannot exceed h_0 , we have at $r = R_t = R/\sqrt{\epsilon_2}$, $h_2(r) = h_0$ and $\epsilon_{\text{eff}} = \epsilon_2$. To achieve an effective dielectric constant of less than ϵ_2 for $R_t \leq r \leq R$, and also to follow the profile given by equation (1), we will use another bilayered medium: one layer is air and the other is also polyethylene. The thickness of the polyethylene plate as function of radius $h_1(r)$ can be determined by the method explained above, leading to

$$h_1(r) = \frac{(R^2 - \epsilon_1 r^2)h_0}{(\epsilon_2 - \epsilon_1)r^2}. \quad (6)$$

It is seen that the curves of $h_1(r)$ and $h_2(r)$ smoothly connect each other at the point $r = R_t$, and the bilayered medium matches with the air ($\epsilon_{\text{eff}} = \epsilon_1 = 1$) at its outermost edge. Finally the variation of the dielectric constant of the device and its material realization are shown in figure 2. For our device, the thickness is $h_0 = 10.0$ mm and for the selected materials we have $R_t = 88.23$ mm and $R_c = 45.36$ mm. The profiles of $h_1(r)$ and $h_2(r)$ from $R_c \leq r \leq R$ determine the shape of the polyethylene plate, which will be cut out by a program-controlled machine.

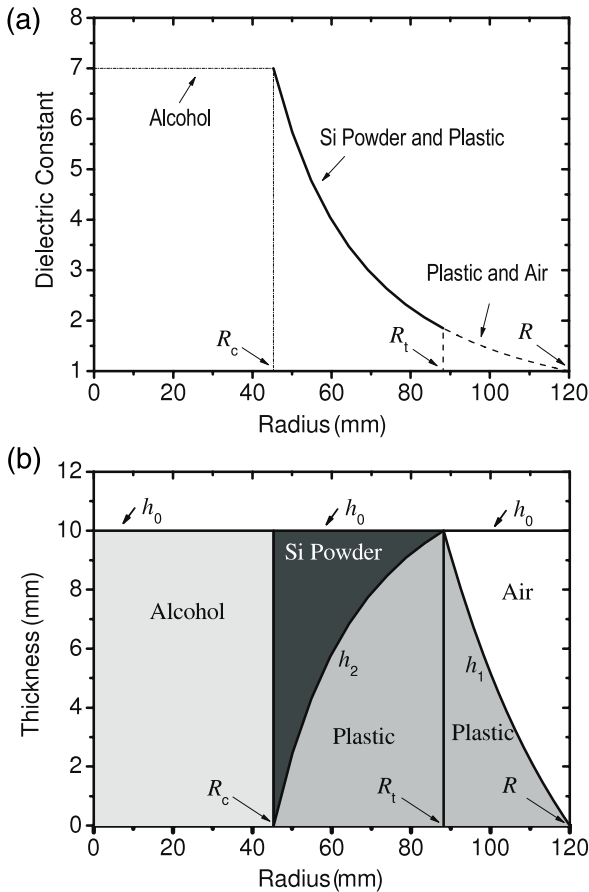


Figure 2. (a) The radius dependent dielectric constant of the omnidirectional electromagnetic absorbing device and (b) its material realization.

3. Experimental implementation

In our experimental setup, the absorbing core is made of a mixture of 29.5% water and 70.5% ethanol and is very dissipative for X-band microwaves. For $R_c \leq r \leq R_t$ the bilayered medium consists of silicon powder with grain size less than $10 \mu\text{m}$ and polyethylene, and for $R_t \leq r \leq R_c$ the bilayer is made of air and the polyethylene. The profile of the polyethylene plate is realized by a program-controlled machine; a picture of the device is shown in figure 3(a). We choose natural silicon powder as the inner shell to match the dielectric constant at the interface of the core, and cut the polyethylene plate with the profile given by $h_1(r)$ and $h_2(r)$. The sample is placed on a thin square aluminum plate of size $120 \text{ mm} \times 120 \text{ mm}$. To fill the liquid mixture, a thin plastic barrel with a wall thickness of 0.1 mm and diameter of $2R_c$ is placed at the central part of the aluminum plate, which contains a mixture of water and ethanol to form the core. Silicon powder is filled in the hollow region formed by the walls of the barrel and the machined polyethylene plate. Figure 3(a) shows the fabricated device.

The device is placed into a chamber between two large parallel aluminum plates. A TEM wave illuminates the device in the chamber, as shown in figure 3(b). X-band microwaves are sent out from one port of the vector network analyzer

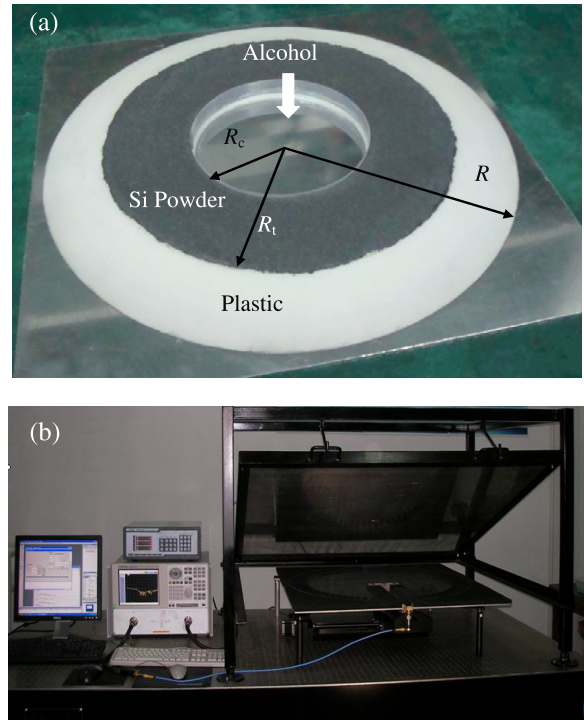


Figure 3. (a) The omnidirectional absorbing device. (b) The electric field mapping system, including an Agilent E8362B vector network analyzer, a $1200 \text{ mm} \times 1200 \text{ mm}$ parallel board waveguide, stepping motor driven translation stage and a main controlling computer.

(Agilent E8362B), and they are incident on the device through a coaxial-waveguide adapter at one edge of the chamber. A coaxial detector is placed on the upper aluminum board; it is coupled with the electric field in the chamber and returns the signals back to the vector network analyzer. The signal is transformed into S_{21} parameter by the analyzer, then the electric field is depicted by the analyzer since its amplitude is linearly scaled to $|S_{21}|$. After calibration, the phase of the electric field can be considered as the same as the measured S_{21} . The lower board of the chamber is monitored by a motor to move in two directions, therefore the detector can scan the electric field on the top of the device. We first calibrate the zero phase by putting the detector closest to the adapter, then we let the detector ‘move’ 0.1 mm by steps near the top of the device; therefore the total electric fields on top of the device are measured.

In order to verify our design, numerical simulations with COMSOL Multiphysics are also performed with frequencies of 9 GHz and 10 GHz at oblique incidence and 10 GHz at normal incidence. The simulation results are shown in figures 4(a)–(c), respectively.

The measured electric field of the omnidirectional absorber at 9.0 GHz is shown in figure 4(d). An electromagnetic beam is incident on the device by the wave adapter at the lower left edge of the parallel Al board. It is clearly observed that the beam follows a bending path when entering the shell of the device. By comparison with the magnitude of the electric fields located inside and outside the device, we can conclude that the main energy stream

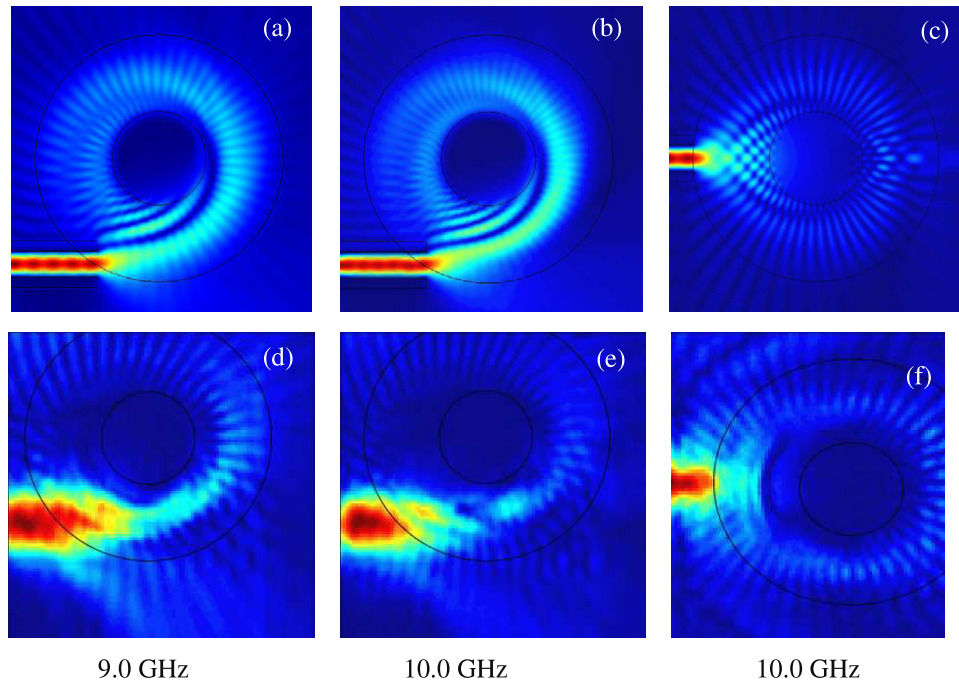


Figure 4. Simulated and measured electric field distributions of the omnidirectional absorbing device. Simulated electric field with oblique incidence at (a) 9.0 GHz and (b) 10.0 GHz, and (c) with normal incidence at 10.0 GHz; measured electric field with oblique incidence at (d) 9.0 GHz and (e) 10.0 GHz, and (f) with normal incidence at 10.0 GHz.

flows within the device and is finally absorbed by the core. The absorption efficiency of the device can be evaluated by comparing the power loss in the device with the incident power. Once the electric field has been measured, the magnetic field at the boundary can also be retrieved as $\vec{H} = i(\nabla \times \vec{E})/\omega\mu$. Therefore, the power loss within the mapped region can be calculated by $P_{\text{loss}} = -0.5 \oint_S \vec{E} \times \vec{H}^* \cdot d\vec{S}$ [19], where S is the borderline of the region. The incident power is obtained simply by calculating the power of the incident beam. Then the absorption efficiency is defined by the ratio of the power loss and the incident power as $\eta = P_{\text{loss}}/P_{\text{in}}$. The measured absorption efficiency of the proposed device is about 81.9%. A little leaked energy is also observed, since the beam travels forward and gradually expands its beam width and the margin of the beam usually carries a small amount of energy. The experimental result compares favorably with the numerical simulation shown in figure 4(a). In the simulation, a relatively thin incident beam was constructed by adapting the waveguide so a clear image of the rotational wave trace is observed; the waves are attracted by the core and they are absorbed. From the contrast of the color inside the device and that of the background, it is found that the amount of leaked energy is low, which is also confirmed by the measured absorption efficiency.

The measured electric field for an oblique incident wave at 10 GHz is shown in figure 4(e). A clearly curved wave trace is also observed, demonstrating the broadband nature of the designed device. A high energy absorbing efficiency (84.9%) is also observed from the field magnitude and distribution. The measured result again agrees with the simulation given by figure 4(b). The electric field distribution of the device under normal incidence was also measured and is shown in

figure 4(f). It is noted that the incident beam is split into several pieces and each travels around the shell and finally falls into the damping core, forming an elliptical-type trajectory. The simulated result shown in figure 4(c) confirms the experimental findings.

Figure 5 shows the measured absorbing efficiency of the designed device within the whole X-band spectrum. The absorption efficiency is as high as over 80% from 9.0 to 12.0 GHz. This demonstrates the broadband nature of the designed device. For an even higher frequency, our device is limited by the frequency dependent dielectric constant of the absorbing material, i.e. alcohol. At 8.0 GHz, the wavelength of the incident wave is relatively large, the width of the beam exceeds the radius of the shell, part of the wave could not fall into the core, and this eventually results in a low absorbing efficiency (58%). This phenomenon also happens at 9.0 GHz (see figure 4(d)); however, it is not very significant. As shown in figure 4(e), a weak field concentration appears due to the small mismatch of impedance at the interface of the absorbing core and the shell. However, this can be alleviated by changing the volume fraction of the ethanol in the alcohol to adapt the real part of its permittivity to match with the silicon powder. The difference between the simulated and experimental results, e.g. the sub-traces shown in figure 4(a) and absent in figure 4(d), is due to the damping factor of the silicon powder, which assimilates part of the stream energy and makes the wave travel a very short way in the shell. Notwithstanding the above deficiency in our measurement, overall, the designed device works successfully in a wide frequency spectrum and is easy to fabricate.

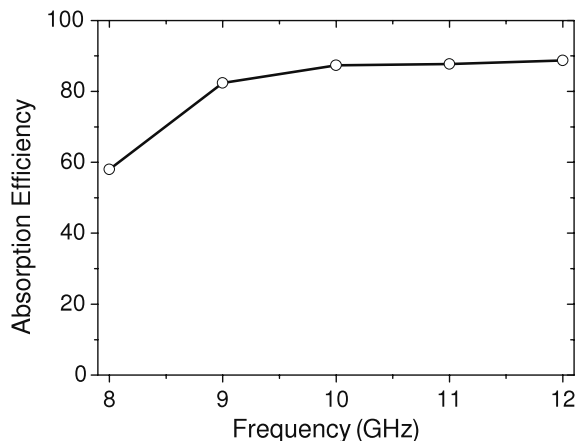


Figure 5. Measured absorption efficiency of the omnidirectional absorbing device within the X-band spectrum. From 9.0 to 12.0 GHz the absorption efficiency is as high as 80% or more.

4. Conclusions

A bilayered structure with classical materials is proposed to realize the electromagnetic omnidirectional absorber reported by Narimanov and Kildishev [18]. The necessary profile of the effective dielectric constant of the device is met by varying the thickness ratio of the bilayered materials as function of the radius. Since the bilayer is made of either silicon powder and polyethylene or air and polyethylene, the device is shown to function in a broadband frequency range. The interaction of the device with an electromagnetic beam is measured by an electric field mapping system, and numerical simulations are also conducted. The measured electric fields agree favorably well with the simulations.

Acknowledgments

This work was supported by the National Natural Science Foundation of China under grant nos 10832002, 11002023, in part by the Doctoral Fund of Ministry of Education of China under grant no. 20091101120004 and BIT Science Foundation under grant no. 20090142011.

References

- [1] Greenleaf A, Lassas M and Uhlmann G 2003 On nonuniqueness for Calderon's inverse problem *Math. Res. Lett.* **10** 685
- [2] Pendry J B, Schurig D and Smith D R 2006 Controlling electromagnetic fields *Science* **312** 1780
- [3] Leonhardt U 2006 Optical conformal mapping *Science* **312** 1777
- [4] Schurig D, Mock J J, Justice B J, Cummer S A, Pendry J B, Starr A F and Smith D R 2006 Metamaterial electromagnetic cloak at microwave frequencies *Science* **314** 977
- [5] Hu J, Zhou X M and Hu G K 2009 Design method for electromagnetic cloak with arbitrary shapes based on Laplace's equation *Opt. Express* **17** 1308
- [6] Ma H, Qu S B, Xu Z, Zhang J Q, Chen B W and Wang J F 2008 Material parameter equation for elliptical cylindrical cloaks *Phys. Rev. A* **77** 013825
- [7] You Y, Kattawar G W, Zhai P W and Yang P 2008 Invisibility cloaks for irregular particles using coordinate transformations *Opt. Express* **16** 6134
- [8] Cai X B, Deng Q B and Hu G K 2009 Experimental study on electromagnetic wave transparency for coated metallic cylinders *J. Appl. Phys.* **105** 103112
- [9] Chen H and Chan C T 2007 Transformation media that rotate electromagnetic fields *Appl. Phys. Lett.* **90** 241105
- [10] Pendry J B, Holden A J, Stewart W J and Youngs I 1996 Extremely low frequency plasmons in metallic mesostructures *Phys. Rev. Lett.* **76** 4773
- [11] Pendry J B, Holden A, Robbins D and Stewart W 1999 Magnetism from conductors and enhanced nonlinear phenomena *IEEE Trans. Microw. Theory Tech.* **47** 2075
- [12] Veselago V G 1968 The electrodynamics of substances with simultaneously negative values of ϵ and μ *Sov. Phys. Usp.* **10** 509
- [13] Shelby R A, Smith D R and Schultz S 2001 Experimental verification of a negative index of refraction *Science* **292** 77
- [14] Cai X B, Zhu R and Hu G K 2008 Experimental study for metamaterials based on dielectric resonators and wire frame *Metamaterial* **2** 220
- [15] Chen H S, Ran L X, Huangfu J T, Zhang X M and Chen K S 2004 Left-handed materials composed of only S-shaped resonators *Phys. Rev. E* **70** 057605
- [16] Caloz C and Itoh T 2006 *Electromagnetic Metamaterials Transmission Line Theory and Microwave Applications* (New Jersey: Wiley)
- [17] Iyer A K, Kremer P C and Eleftheriades G V 2003 Experiment and theoretical verification of focusing in a large, periodically loaded transmission line negative refractive index metamaterial *Opt. Express* **11** 696
- [18] Narimanov E E and Kildishev A V 2009 Optical black hole: Broadband omnidirectional light absorber *Appl. Phys. Lett.* **95** 041106
- [19] Cheng Q, Cui T J, Jiang W X and Cai B G 2010 An omnidirectional electromagnetic absorber made of metamaterials *New J. Phys.* **12** 063006
- [20] Lu W L, Jin J F, Lin Z F and Chen H Y 2010 A simple design of an artificial electromagnetic black hole *J. Appl. Phys.* **108** 064517